Catalysis Letters 30 (1995) 279–288

Oxidative dehydrogenation of 1-butene to butadiene on α-Fe_2O_3/$ZnAl_2O_4$ and $ZnFe_xAl_{2-x}O_4$ catalysts

J.A. Toledo, M.A. Valenzuela, H. Armendáriz, G. Aguilar-Ríos, B. Zapata, A. Montoya, N. Nava, P. Salas and I. Schifter

Instituto Mexicano del Petróleo, SGIDTTI, Eje Central L. Cárdenas No. 152, A.P. 14-805, CP 07730, Mexico D.F., Mexico

Received 7 January 1994; accepted 13 October 1994

The oxidative dehydrogenation of 1-butene to butadiene was studied over a series of catalysts of iron impregnated on $ZnAl_2O_4$ used as a support and also Fe coprecipitated with zinc and aluminum in order to obtain $ZnFe_xAl_{2-x}O_4$ type catalysts. Results were compared with bulk α-Fe_2O_3, $ZnAl_2O_4$ and $ZnFe_2O_4$. X-ray diffraction (XRD) and Mössbauer spectroscopy suggest that in the impregnated catalysts, Fe ions are in strong interaction with the support. These samples have higher butadiene selectivity than coprecipitated $ZnFe_xAl_{2-x}O_4$ catalysts, in which iron is incorporated into the $ZnAl_2O_4$ spinel network. Results suggest also that iron content has a greater effect on butadiene selectivity than the zinc aluminate–iron oxide interaction.

Keywords: oxidative dehydrogenation; α-Fe_2O_3; oxide supported catalysts; $ZnAl_2O_4$ spinel structure; Mössbauer spectroscopy, XRD

1. Introduction

Unsupported iron-based catalysts have been widely used in the oxidative dehydrogenation of 1-butene to butadiene, hematite (α-Fe_2O_3, with corundum type structure) has been reported to be a very active catalyst but non-selective [1–3].

Several studies indicated that supporting α-Fe_2O_3 on a high surface area carrier influences its catalytic properties [4,5]. Part of those works were centered around the so-called strong metal–support interaction (SMSI), which is manifested, for instance, by a marked decrease in hydrogen and carbon monoxide adsorption [6]. Moreover, it has been established that α-Fe_2O_3 crystallite size has a marked effect on butadiene selectivity [7].

In order to investigate the interaction between metal oxide and support, two series of catalysts were studied: one was iron oxide supported on zinc aluminate (α-Fe_2O_3/$ZnAl_2O_4$) prepared by impregnation, and the other one was zinc-iron aluminate ($ZnFe_xAl_{2-x}O_4$) synthesized by a coprecipitation method. Both series of

catalysts were evaluated in the 1-butene oxidative dehydrogenation and compared with bulk α-Fe_2O_3, $ZnAl_2O_4$ and $ZnFe_2O_4$.

2. Experimental

2.1. CATALYST PREPARATION

Zinc aluminate support ($ZnAl_2O_4$) was prepared by the coprecipitation method from nitrate parent salts at 50°C and variable pH (from 2 to 7.5). $(NH_4)_2CO_3$ (23 wt% aqueous solution) was used as precipitating agent. The obtained gel was washed with doubly distilled water, filtered and dried overnight at 110°C in a vacuum oven and later calcined in two steps: first at 400°C for 4 h, and then at 800°C for 4 h, in air flow (20 cm^3/min).

The catalysts of series I were obtained by impregnation of $ZnAl_2O_4$ with a $Fe(NO_3)_3 \cdot 9H_2O$ alcoholic solution, excess of alcohol was evaporated at 70°C for 4 h in a rotatory evaporator. The resulting samples were calcined in air flow (20 cm^3/min) at 500°C for 0.5 h, then at 800°C for 4 h. These samples were labeled I*n*, where *n* represents the nominal amount of iron in the catalyst (table 1).

$ZnFe_xAl_{2-x}O_4$ catalysts were prepared by the coprecipitation method (series C) from an aqueous solution of the corresponding nitrates. The precipitation was carried out with an aqueous solution of NH_4OH at 50°C and variable pH (from 2 to 7.5). The obtained gels were carefully washed with doubly distilled water, filtered and dried at 110°C overnight in a vacuum oven. Calcination was carried out in air flow (30 cm^3/min) at 800°C for 6 h. These samples were labeled as C*n*, where *n* represents, again, the iron concentration (table 1).

2.2. CHEMICAL ANALYSIS

The chemical composition of the prepared catalysts was determined by atomic absorption spectroscopy in a Perkin Elmer apparatus.

Table 1
Chemical composition and lattice parameters

Catalyst	Elemental composition (wt%)			Atomic ratio (Fe + Al)/Zn	Lattice parameter (Å)
	Fe	Al	Zn		
I1	0.79	27.05	33.37	2.00	8.095
I5	5.15	27.05	33.27	2.15	8.105
I8	8.06	27.05	33.27	2.25	8.105
C1	1.49	28.95	34.89	2.06	8.099
C5	4.96	26.96	34.38	2.07	8.120
C8	8.34	24.15	33.06	2.07	8.130

2.3. TEXTURAL PROPERTIES

Nitrogen physisorption data of the catalysts were obtained on a Micromeritics ASAP-2000 apparatus.

2.4. X-RAY DIFFRACTION (XRD)

X-ray diffraction patterns were obtained on a Phillips diffractometer equipped with a Mo anode and a secondary beam monochromator of graphite crystal in order to guarantee Kα radiation. Cell parameters were measured using the (113) reflection plane of α-Al_2O_3 as an internal standard.

2.5. MÖSSBAUER SPECTROSCOPY

Mössbauer spectra of the catalysts were obtained on a conventional constant-acceleration spectrometer Austin-5600 with krypton proportional detector. The γ-ray source was ^{57}Co in a rhodium matrix of 25 mCi. Laser velocity calibration was performed using an iron foil as reference. A standard least-squares minimization routine was used to fit the spectra as a superposition of Lorentzian lines.

2.6. CATALYTIC ACTIVITY

The oxidative dehydrogenation reaction was carried out in a conventional continuous flow system at atmospheric pressure (590 mm Hg). A mixture of 5 mol% of 1-butene (Matheson C.P.), 5 mol% of oxygen (Linde 99.6% purity) and 90 mol% of helium (Linde 99.6% purity) was fed to the reactor. The total flow rate was 60 cm^3/min and 0.2 g of catalysts were used for each test, reaction was performed at 420°C and products of reaction analyzed using on-line gas chromatography. Details of the reaction system and analysis are published elsewhere [8].

3. Results and discussion

3.1. CHEMICAL COMPOSITION

Table 1 shows chemical composition and cell size of the prepared catalysts; both series present a similar iron loading. In C*n* samples a decrease in Al content was observed, with an atomic ratio (Fe + Al)/Zn of about 2.

3.2. TEXTURAL PROPERTIES

Table 2 shows BET surface area (SA), pore volume (PV) and average pore diameter (APD). Impregnated catalysts show a BET surface area around 23 m^2/g with very little changes among them. As iron content increases, PV and APD increase

Table 2
Textural properties of the catalysts

Catalyst	Surface area (m^2/g)	Pore volume (cm^3/g)	Average pore diameter (Å)
II	22.62	0.1350	238.74
I5	23.47	0.1516	258.40
I8	26.21	0.4066	620.45
C1	12.15	0.5320	494.88
C5	20.58	0.1546	300.52
C8	83.45	0.3048	146.10

also. Considering coprecipitated catalysts, textural properties follow a different behavior: SA increases dramatically as iron content increases (12–83 m^2/g). Moreover, pore size distribution is monomodal, while impregnated catalysts show a bimodal pore size distribution (fig. 1). These textural differences give a first evidence that suggests two types of catalysts: one with α-Fe_2O_3 on $ZnAl_2O_4$ surface and the other with iron ions incorporated into the $ZnAl_2O_4$ spinel network.

3.3. X-RAY DIFFRACTION (XRD)

The X-ray diffraction patterns, for both series of catalysts showed the characteristic pattern of $ZnAl_2O_4$ spinel structure (JCPDS 5-669). In spite of the fact that

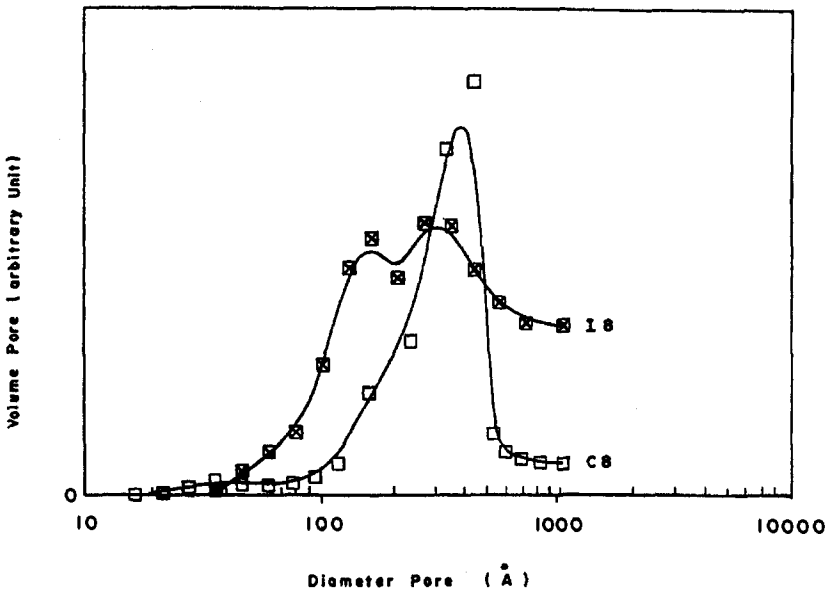

Fig. 1. Pore size distribution of the samples I8 (8.06 wt% Fe on $ZnAl_2O_4$) and C8 (8.34 wt% Fe in $ZnFe_xAl_{2-x}O_4$).

iron content was high (5.15 wt% in catalyst I5, and 8.06 wt% in catalyst I8), α-Fe_2O_3 was not observed. In table 1, cell parameters of the cubic spinel structure for both series of catalysts are shown. For the coprecipitated catalysts, a gradual increase in $ZnAl_2O_4$ cell size with iron content is observed, following Vegard's law, which is an accordance with molecular dimensions: $ZnFe_2O_4$ has a larger cell size (8.441 Å, JCPDS 22-1012) than $ZnFe_2O_4$ (8.081 Å, JCPDS 5-669). This fact would explain the greater increase in SA as iron content increases in coprecipitated catalysts. By contrast, in the impregnated catalysts the cell size remains constant, which could be indicative that there are no substitutions of Al^{3+} by Fe^{3+} in the octahedral sites of the spinel structure. To explain the absence of XRD patterns from the α-Fe_2O_3 phase in the I*n* series one can consider very dispersed iron ions occupying the octahedral vacancies into the spinel surface [9].

In the impregnated catalysts, the iron oxide is suspected to form very small particles [10], not detected by XRD. In coprecipitated catalysts we assume (according to the preparation method and cell parameters variation) that iron is located inside $ZnAl_2O_4$ spinel structure forming $ZnFe_xAl_{2-x}O_4$ type compounds, in which Al^{3+} is replaced by Fe^{3+} in an isomorphic way. In order to follow the thermal behavior of the catalysts, the samples I8 and C8, with the highest iron content, were treated at 1000°C in air flow (30 cm^3/min) during 4 h. The X-ray diffraction patterns for these samples are shown in fig. 2. It can be noticed that in sample I8, the α-Fe_2O_3 phase has been segregated, which is evidenced by the peak located at $2\theta = 15.1°$, while in sample C8 only the diffraction peaks corresponding to the zinc aluminate structure were identified. In addition, zinc aluminate stabilizes the coprecipitated iron oxide against sintering.

3.4. MÖSSBAUER SPECTROSCOPY

Fig. 3 shows the room-temperature Mössbauer spectra obtained at ±10 mm/s velocity. The magnetically split sextuplet, caused by big particles of α-Fe_2O_3 was not observed. With respect to impregnated catalysts, sample I1 shows a singlet near to zero velocity, characteristic of very small α-Fe_2O_3 particles with high dispersion [4,10], probably due to the lowest iron content (0.79 wt% Fe). Notice also that, at high driver velocity, the resonance zone is not well resolved because the background dispersion overlaps with the absorption peaks of the spectra.

In samples I5 and I8, a well resolved doublet was observed, attributed to Fe^{3+} ions in octahedral sites in a normal spinel structure [8] and to very small silica supported α-Fe_2O_3 particles having superparamagnetic behavior [11,12].

In the case of the coprecipitated catalysts a doublet near zero velocity is observed in all samples. Sample C1 presents a central doublet with non-lineal experimental data dispersion, which could be associated to the presence of α-Fe_2O_3 species [10]. In order to obtain a better resolution of the resonance zone, the driver velocity was lowered to ±2 mm/s. The improved spectra are shown in fig. 4. The parameters used to fit the spectra are summarized in table 3. The isomer shifts (IS)

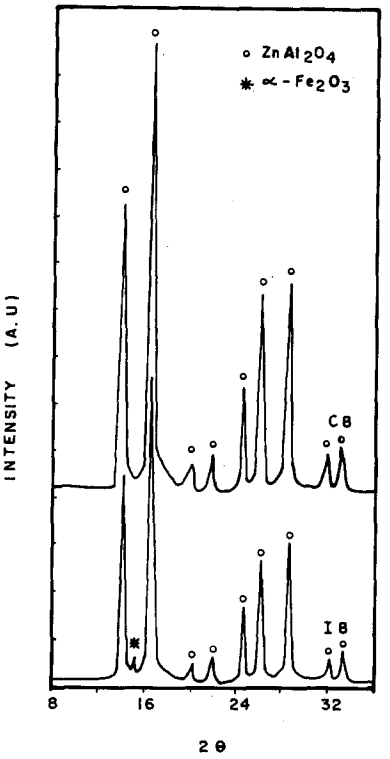

Fig. 2. X-ray diffraction of the samples I8 and C8, treated at 1000°C in air flow (30 cm^3/min) during 4 h.

are all consistent with Fe^{3+}. Impregnated and coprecipitated catalysts showed only a superparamagnetic pattern consistent of a centered doublet. The Fe^{3+} doublet with the higher quadrupole splitting can be assigned to iron in strong interaction with the support [12]. In particular, the quadrupole splitting has been found to increase with decreasing crystallite size [12,13]. For both series of catalysts high quadrupole splittings are obtained with respect to $ZnFe_2O_4$ and $ZnCr_xFe_{2-x}O_4$ reported elsewhere [8,14]. The higher values were obtained for impregnated catalysts with different tendencies with respect to iron content: For impregnated catalysts quadrupole splitting decreases as iron content is increased leading to growing iron particles. In contrast, for coprecipitated catalysts quadrupole splitting increases with iron content (decreasing size of iron particles). This behavior was attributed to $ZnAl_2O_4$ lattice distortion as a consequence of isomorphic substitution of Al^{3+} by Fe^{3+}. Dumesic and Topsøe [15] have pointed out that lattice distortion, which extended to the surface, has an important contribution to quadrupole splitting. These arguments can be used to explain the absence of α-Fe_2O_3 particles in both series of catalysts. Considering that in both series of catalysts the isomer shifts and quadrupole splitting are similar, we assume that Fe^{3+}

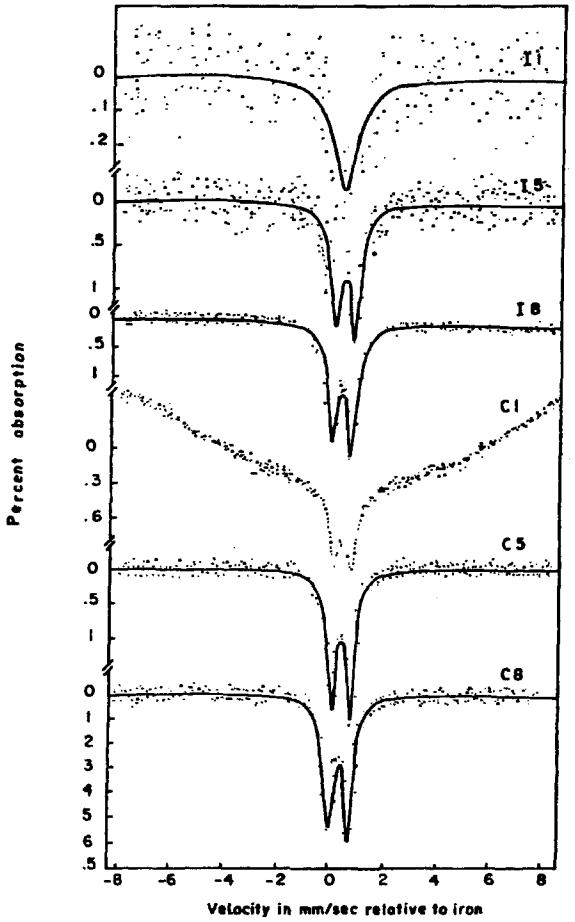

Fig. 3. Mössbauer spectra of the impregnated (I*n*) and coprecipitated (C*n*) catalysts obtained at ±10 mm/s, room temperature.

ions are found in octahedral sites; in the I*n* series remaining in the *natural* octahedral vacancies in the spinel structure surface and in the C*n* series occupying the octahedral sites corresponding to Al^{3+} ions in the spinel structure network. In both cases the Fe^{3+} ions are found in a very dispersed state.

3.5. CATALYTIC ACTIVITY

Table 4 summarizes activity and selectivity data at 420°C measured at 1 h on stream. In a 3 h reaction period no deactivation of the catalysts was detected, as comparison, data for α-Fe_2O_3 pure $ZnAl_2O_4$ and $ZnFe_2O_4$ phases are also included. It can be seen that, although the reaction data were obtained under somewhat different conversions, impregnated catalysts showed higher butadiene selectivity than coprecipitated catalysts and unsupported α-Fe_2O_3. Moreover, pure

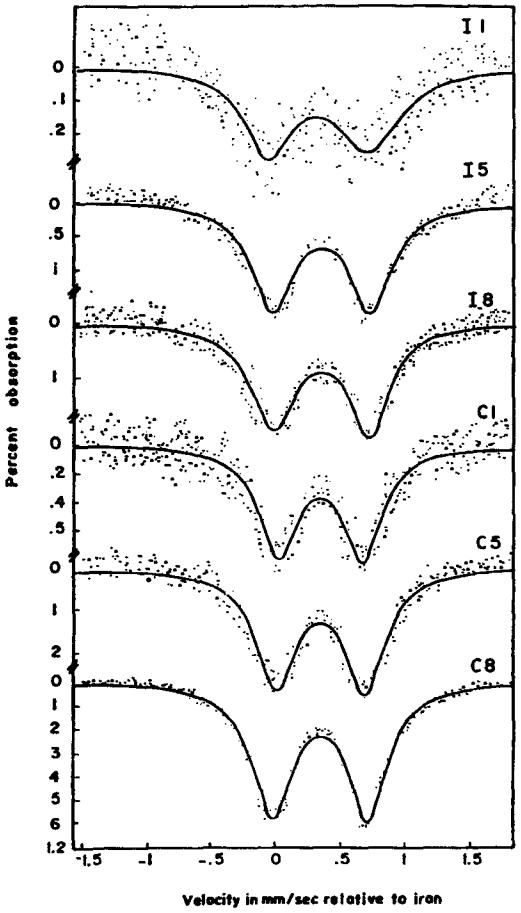

Fig. 4. Mössbauer spectra of the impregnated (I*n*) and coprecipitated (C*n*) catalysts obtained at ±2 mm/s, room temperature.

Table 3
Mössbauer parameters of the catalysts

Catalyst	IS [a] (mm/s)	QS [b] (mm/s)	$\Gamma/2$ [c] (mm/s)
I1	0.3257	0.7599	0.2504
I5	0.3581	0.7525	0.1938
I8	0.3524	0.7278	0.1976
C1	0.3522	0.6344	0.1441
C5	0.3520	0.6866	0.1888
C8	0.3485	0.7322	0.1811

[a] IS: isomer shift relative to iron foil.
[b] QS: quadrupole splitting.
[c] $\Gamma/2$: half linewidth.

Table 4
Catalytic activity and selectivity for the 1-butene oxidative dehydrogenation [a]

Catalyst	Conversion (%)	Selectivity (%)			
		butadiene	CO_2	cracking	butenes
I1	32.94	11.38	15.78	0.94	71.89
I5	36.45	41.59	29.38	0.68	28.34
I8	52.31	56.29	23.99	0.42	19.27
CI	22.68	22.15	21.03	1.19	45.85
C5	46.33	34.25	21.43	0.71	43.60
C8	45.63	51.45	23.99	0.00	24.54
α-Fe_2O_3	55.56	36.07	28.15	0.00	35.78
$ZnFe_2O_4$	16.92	78.66	12.41	0.00	8.92
$ZnAl_2O_4$	32.01	1.31	3.11	0.75	94.81

[a] Reaction temperature: 420°C; feed: 5% 1-butene, 5% oxygen in helium; catalyst weight: 0.200 g.

$ZnAl_2O_4$, although it shows high activity towards 1-butene isomerization to 2-butenes, does not present activity to dehydrogenation. $ZnFe_2O_4$ shows low activity but the highest selectivity to butadiene. In both series of catalysts the 1-butene conversion and selectivity to butadiene increase with iron content. The increase in activity with iron content can be attributed to a more dispersed iron phase instead of sintered aggregates. As it can be seen, Fe^{3+} in $ZnFe_2O_4$ spinel structure is the more selective to butadiene formation which leads us to think about an increasing formation of iron ions with a similar environment as in $ZnFe_2O_4$ structure as iron content is increased, no matter the preparation method employed. Note that in C8 and I8 samples the selectivity values are very similar.

4. Conclusions

Catalytic activity is proportional to iron content when impregnation or coprecipitation methods are employed. Selectivity to butadiene is higher when the impregnation method is used, except for low iron content.

When catalysts are prepared by coprecipitation, iron ions are incorporated into the zinc aluminate spinel network, whereas for impregnated samples iron ions occupy octahedral vacancies on the $ZnAl_2O_4$ spinel surface.

References

[1] B.L. Yang, D.S. Cheng and S.B. Lee, Appl. Catal. 70 (1991) 161.
[2] M. Zhang, R. Lan, J. Liu, X. Chen and W. Zhov, J. Chem. Soc. Faraday Trans. 88 (1992) 637.
[3] B.L. Yang, M.C. King and H.H. Kung, J. Catal. 89 (1984) 172.
[4] T. Yoshioka, J. Koezuka and H. Ikoma, J. Catal. 16 (1980) 242.

[5] C.R.F. Lund and J.A. Dumesic, J. Phys. Chem. 86 (1982) 130.
[6] D.G. Rethwisch and J.A. Dumesic, J. Phys. Chem. 90 (1986) 1863.
[7] B.L. Yang, F. Hong and H.H. Kung, J. Phys. Chem. 88 (1984) 2531.
[8] H. Armendariz, G. Aguilar-Ríos, P. Salas, M. Valenzuela and Y. Schifter, Appl. Catal. 92 (1992) 29.
[9] N.N. Greenwood, *Cristales Ionicos, Defectos Reticulares y no Estequiometría* (Alhambra, S.A., 1979) p. 70.
[10] D.P. Hoffman, M. Hovalla, A. Proctor, M.J. Fay and D.M. Hercules, Appl. Spectry. 46 (1992) 208.
[11] T. Ida, H. Tsuiki, A. Veno, K. Thoji, Y. Udayawa, K. Iwai and H. Sano, J. Catal. 106 (1987) 428.
[12] F. Hong, B.L. Yang, L.H. Schwartz and H.H. Kung, J. Phys. Chem. 88 (1984) 2525.
[13] H.M. Gager and M.C. Hobson Jr., Catal. Rev. Sci. Eng. 11 (1975) 117.
[14] H. Armendáriz, J.A. Toledo, M.A. Valenzuela, G. Aguilar R., P. Salas, A. Cabral, H. Jiménez and I. Schifter, J. Mol. Catal. 92 (1994) 325.
[15] J.A. Dumesic and H. Topsøe, Adv. Catal. 26 (1977) 121.